Laser-Controllable Coatings for Corrosion Protection

Ekaterina V. Skorb,[†,‡,*] Andre G. Skirtach,[†] Dmitry V. Sviridov,[‡] Dmitry G. Shchukin,[†] and Helmuth Möhwald[†]

[†]Max Planck Institute of Colloids and Interfaces, Am Mühlenberg 1, 14424, Potsdam, Germany, and [‡]Institute for Physico-Chemical Problems of Belarusian State University, Minsk, Belarus

ABSTRACT We introduce a novel and versatile approach to the corrosion protection by use of "smart" laser-controllable coating. The main advantage of the proposed technique is that one could terminate the corrosion process by very intensive healing after an appearance of corrosion centers using local laser irradiation. It is also shown that by applying a polyelectrolyte shell with noble metal particles over the mesoporous titania and silica *via* layer-by-layer assembly it is possible to fabricate micro- and nanoscaled reservoirs, which, being incorporated into the zirconia—organosilica matrix, are responsible for the ability of laser-driven release of the loaded materials (*e.g.*, corrosion inhibitor). Furthermore, the resultant films are highly adhesive and could be easily deposited onto different metallic substrates. Laser-mediated remote release of incorporated corrosion inhibitor (benzotriazole) from engineered mesoporous containers with silver nanoparticles in the container shell is observed in real time on single and multicontainer levels.

KEYWORDS: laser regulation · light-stimulated · release · containers · corrosion healing

The importance of corrosion protection does not need to be emphasized. The most widely used and effective anticorrosion coatings are those based on using hexavalent chromium.[1−4] However, the use of Cr(VI) is becoming increasingly restrictive due to its characteristic as human carcinogen and substantial contribution to environmental pollution. Organically modified silicates are hybrid organic−inorganic materials formed through hydrolysis and condensation of organically modified silanes with traditional alkoxide precursors and could be used as an alternative to the traditional anticorrosion coatings based on Cr(VI).[5−9] These coatings exhibit increased flexibility and adhesion in comparison with their inorganic counterparts. In general, the sol−gel-derived coatings have been found to provide good corrosion resistance for metal substrates because of their barrier properties, tenacious adhesion to metal substrates, chemical inertness, versatility in coating formulations, and ease of application under ambient temperature conditions.[10−12] The greatest disadvantage of individual sol−gel hybrid films is the absence of healing the corrosion centers after their appearance. Such healing becomes possible when corrosion inhibitor is directly incorporated into the hybrid sol−gel matrix.[13,14] Another approach preventing corrosion propagation on metal surfaces uses a corrosion reaction to initiate inhibitor action (*i.e.*, the corrosion process itself can be a stimulus triggering the release of corrosion inhibitors from the coating). A few coatings with so-called self-healing effect were explored up to now.[15] Ion-exchange resins can release inhibitors in response to reactions with corrosive ions.[16] Monomer-filled capsules introduced into polymer coatings are capable of healing the defects in the coating by releasing encapsulated monomer followed by polymerization and sealing of the defected area.[17]

The main goal of this study is the development of novel "smart" remotely controlled corrosion protection coatings, which radically improve the long-term performance of metallic substrates. We present a new mechanism based on the healing ability of anticorrosion agents remotely activated by laser. Remote laser-induced release demonstrates a facile method of controlling the properties of substrate coatings and improved performance. The ability to remotely release the loaded material is important in delivery of chemicals and in biomedical application areas.[17−19] Using laser technology, the method relies on making the containers sensitive to light by doping them with metal nanoparticles or organic dyes.[20−22] Upon laser light illumination, the absorption centers locally disrupt the shells of the containers, thus increasing the permeability of the container walls. The inhibitor stored in the container is then released covering and healing the corrosion

*Address correspondence to skorb@mpikg.mpg.de.

Received for review April 6, 2009 and accepted June 24, 2009.

Published online July 2, 2009.
10.1021/nn900347x CCC: $40.75

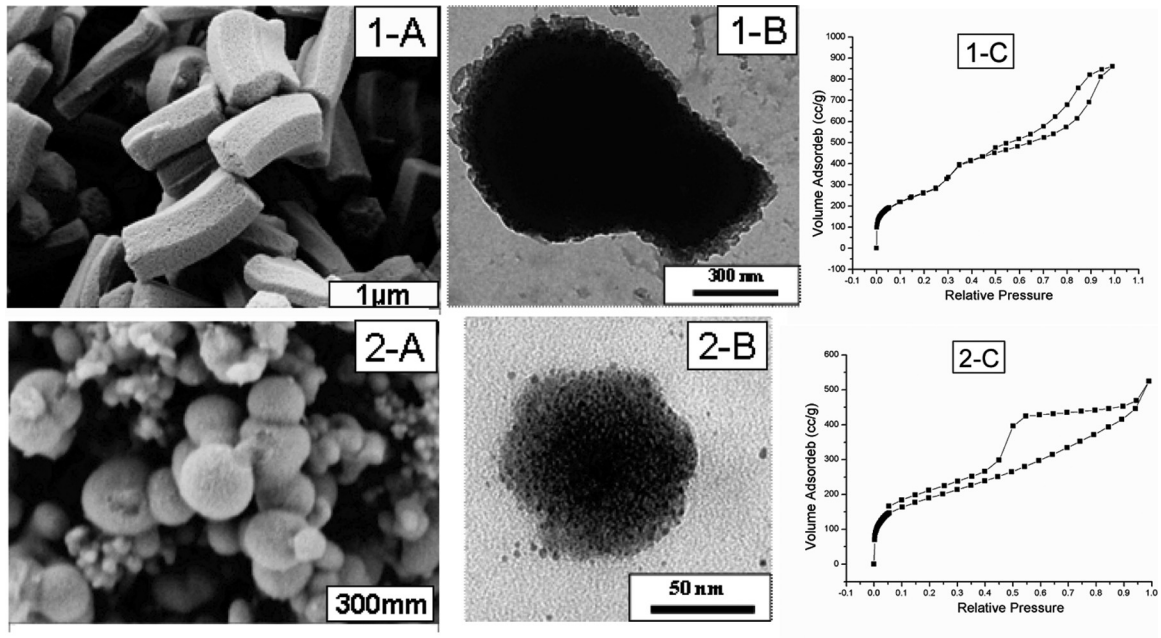

Figure 1. (1-A) SEM image of porous SiO_2 particles. (1-B) TEM image of porous SiO_2 particle with polyelectrolyte layers and silver particles incorporated into the polyelectrolyte shell. (2-A) SEM image of porous TiO_2 particles. (2-B) TEM image of titania particle modified by nanosized photodeposited silver particles. (C) Adsorption isotherms of (1) SiO_2 and (2) TiO_2 porous particles.

area. In the long run, the use of polyelectrolyte shell made *via* layer-by-layer polyelectrolyte deposition and incorporation of the resultant containers into sol−gel film allows successful development of corrosion protective systems with reservoirs for corrosion inhibitor. Silver nanoparticles can be used as light absorption centers because of their strongly pronounced surface plasmon resonance band. The surface plasmon resonance of silver nanoparticles is located at ~420 nm, inducing their aggregation, and sufficient absorption can be made in the broad visible−near-IR wavelength range. The surface plasmon resonance of silver nanoparticles is located at ~420 nm, while for gold nanoparticles, it is at ~520 nm. Aggregation of nanoparticles induces absorption in the near-infrared part of the spectrum due to interacting dipole moments on neighboring nanoparticles. That opens new possibilities for remote regulation of corrosion healing. Interchange of various wavelengths that can be used for remote activation is important. Typically, one would use visible laser light hitting the absorption maximum of metal nanoparticles. However, adding the possibility of application of near-IR light makes this method rather flexible.

It is important to emphasize the fact that remote activation of containers makes the proposed approach versatile. Indeed, one anticipates that activation could be performed without further inspection: the surface could be periodically exposed to laser light. If a scratch or other defects occur and the surface becomes prone to corrosion, then illumination by laser light would ensure that these defects have been cured. In this regard, such coatings behave as "smart" ones because they initiate triggering of release at defined surface areas including the corrosion pit; otherwise, the corrosion protection containers just stay nonactivated under the coating and do not initiate any action.

RESULTS AND DISCUSSION

The hybrid SiO_x:ZrO_x-based coatings were initially developed for corrosion protection of metals.[10−12,15] Notwithstanding the fact that these films are highly corrosion protective, they have one main disadvantage: the absence of corrosion healing and, consequently, termination of a corrosion process. It should be noted that, together with the formation of protective coating, these films are subjected to crack appearance because of physical or chemical influences, for example, small stone scratches or chloride ion attack, and as a result, corrosion starts. We have found a way to heal the corrosion centers in a sol−gel film after their appearance. For this purpose, two types of mesoporous containers with corrosion inhibitor (benzotriazole) entrapped inside the pore volume were synthesized (Figure 1). Both types of containers, submicrometer silica and nanosized titania, were investigated: the advantage of the first one is the higher quantity of corrosion inhibitor, which could be incorporated into free pore volume; the advantage of the other is the smaller container size which allows their incorporation into very thin films. Both SiO_2 and TiO_2 powders show a large BET specific surface area reaching 864 and 529 m^3/g, respectively (Figure 1 (1C,2C)). The BET isotherm allows derivation of the pore size distribution. The pores are distributed in a narrow range, and the average pore size is about

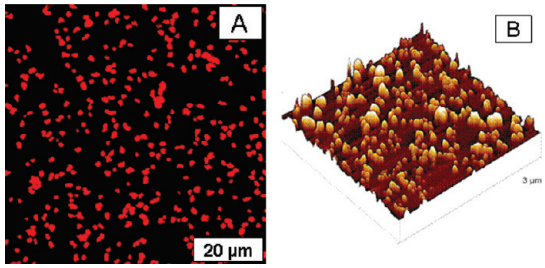

Figure 2. Confocal and AFM images of containers incorporated into sol−gel film: (A) confocal fluorescence image of SiO_2 containers (the Rhodamine 6G is incorporated into pores); (B) AFM surface data for mesoporous TiO_2-loaded SiO_x:ZrO_x film.

~7 nm in the case of TiO_2 and ~17 nm in the case of silica.

The technique of layer-by-layer (LbL) deposition of oppositely charged species (*e.g.*, synthetic and natural polyelectrolytes, biomaterials, metal, and inorganic nanoparticles) on the titania or silica core enables the stepwise assembling of ordered multilayers with nanometer-scale precision.[23] This approach yields reservoirs with controllable storage/release properties because the permeability of the polyelectrolyte shell can be changed by varying pH, ionic strength of the medium, or other physical or chemical influence.[24,25] Selective and variable permeability of polyelectrolyte containers toward large organic molecules, polymer molecules, and nanoparticles makes them an efficient transport tool for protection, delivery, and storage of active species and substances with unstable formulation.[26,27] The reinforcement of polyelectrolyte walls with noble metal nanoparticles imparts them sensitivity in the visible and near-IR spectral regions and, in its turn, to exert remote control over their release properties.[18,20,28,29] The TEM images show silica containers with polyelectrolyte shell, silver particles being incorporated into the shell (Figure 1(1-B)) and titania nanosized mesoporous particles after photodeposition of silver particles from silver nitrate 10^{-5} M solution under UV irradiation (Figure 1(2-B)). The containers were added to zirconia sol that was then mixed with organosiloxane sol, and the obtained mixture was used for film deposition. The confocal and AFM images of the resultant film (Figure 2) evidence uniform distribution of the containers over the coating. The concentration of the silica-based containers, as evidenced by the confocal image Figure 2A, is ~10^7 containers/m^2. The AFM image of TiO_2-loaded sol−gel film (Figure 2B) shows that concentration of the titania-based container is ~10^{11} containers/m^2. That uniform distribution and high surface concentration of containers allows effective healing of the damaged corrosion area. Here, we offer to use both visible and IR laser irradiation to heal the corrosion defects. This enables the release of corrosion inhibitor after a short-term exposure to the laser light by switching the permeability of the containers. In case of a pulsed laser beam, the release occurs after exposure to a single pulse, although scanning of the spot can be used to increase the illumination area. In the case of continuous laser operation, the release was triggered on an area of ~1 mm^2 during a single exposure in the seconds interval time. Reaching larger areas is possible by scanning the affected area with the laser beam.

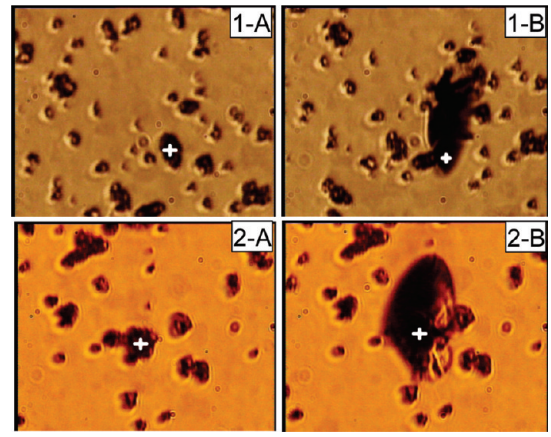

Figure 3. Images (bright field mode) (1) SiO_2 containers modified with silver nanoparticles and (2) titania modified with silver nanoparticles. The images are obtained before (A) and after (B) local illumination with an IR laser beam (white cross shows the position of the IR laser beam). The particles correspond to aggregates of nanocontainers. Inside the container pore is incorporated Rhodamine 6G dye.

The laser effect on containers is the following: the surface plasmon resonance of noble metal nanoparticles is located in the visible and near-IR part of the spectrum. Therefore, light energy is converted into heat energy upon laser light illumination. Heat absorption can be high, and it can affect the polymeric shells. In earlier work, various metal nanoparticles including silver, gold and gold sulfide, and gold nanorods were tested.[28,29] They were shown to affect the permeability of the polymeric shell, resulting in release of encapsulated materials. These remote-release experiments were conducted according to the following scheme. The polyelectrolyte multilayer shell or container cores were modified with metal nanoparticles, which served as absorption centers for energy supplied by a laser beam. These absorption centers cause local heating that disrupts the local polymer shell and allows the loaded corrosion inhibitor to leave the interior of the containers. Very important parameters that control the interaction of laser light with the absorption centers are the size of the nanoparticles and their concentration. The concentration of metal nanoparticles plays an important role for two reasons: (1) when the distance between the two adjacent nanoparticles is of the order of their size, the thermal effects produced by adjacent nanoparticles add up; and (2) the interaction of nanoparticles located in close proximity to each other results in an increase of absorption at lower energies or higher wavelengths (causing the so-called red shift) compared to the surface plasmon resonance band of stand-alone

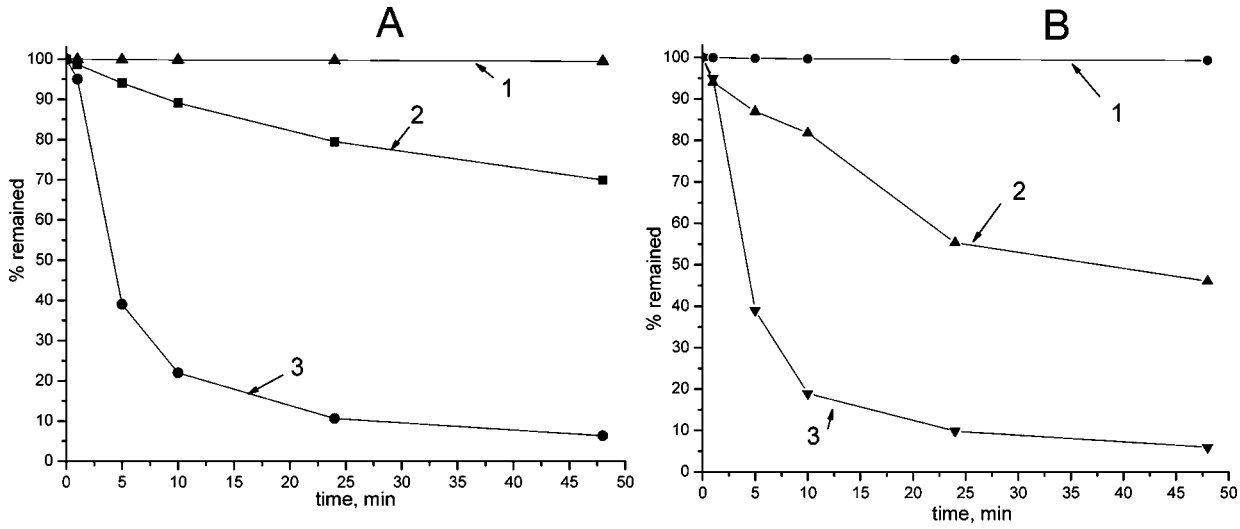

Figure 4. Release of benzotriazole from (A) SiO_2/Ag, (B) TiO_2/Ag containers with polyelectrolyte shell at (1) pH = 7, (2) pH = 10.1, and (3) under IR laser irradiation.

nanoparticles.[30−32] In this regard, spatial arrangement of the nanoparticles is essential, and control of their distribution is paramount.[33−36] In the present studies, we used silver nanoparticles for the remote activation of containers. These nanoparticles were chosen because of their superb surface plasmon resonance absorption. The average size of silver nanoparticles was ~8 nm. Further studies were conducted on the release of the corrosion inhibitor from the containers upon laser illumination that should result in the termination of the corrosion process. The surface plasmon resonance of noble metal nanoparticles and their aggregates is located in the visible and near-IR part of spectrum.

As was mentioned earlier, upon exposure to laser light, the nanocontainers ruptured, releasing their contents. It is apparent from the images that were recorded in transmission mode before and after illumination (Figure 3) that the containers can be opened in a light-addressable mode, and the release of the encapsulated luminescent dye (Rhodamine 6G) can be thus obtained (Video 1S in Supporting Information). The observed effect can be attributed to the photothermal conformation change of the polyelectrolyte shell resulting in its switching to the opening state.[37] Thus, the rupture of the containers demonstrates that a laser−nanoparticle interaction through a thermal processes is responsible for container activation.[37] Other processes, for instance, transport of protons or electron redistribution around the nanoparticles,[38] do not determine the activation of the containers because the polyelectrolyte multilayers were shown to be permeable for protons and the local redistribution of electrons cannot cause the rupture of the containers.[39] Notably, the rise in temperature during laser illumination of containers with embedded nanoparticles is several degrees, and it is concentrated in the vicinity of the containers.[29] In our earlier work, we measured the temperature increase upon laser illumination of polymeric microcapsules containing gold and gold−sulfide nanoparticles.[28] It was found that such parameters as the size of nanoparticles, their concentration, and incident intensity affect the temperature rise in the vicinity of the nanoparticles. Concentration of nanoparticles is a parameter that can be easily controlled by the deposition conditions. In the case when the substrate is illuminated by a laser operating at the wavelength in close proximity of the surface plasmon resonance, a single absorbing nanoparticle will provide sufficient temperature rise for release of encapsulated inhibitors, with the temperature rise on that nanoparticle being controllable by the intensity of the laser beam. When illumination is performed in the near-IR part of the spectrum, the concentration of nanoparticles and their aggregation state, in particular,[18] play an important role. Indeed, closely located nanoparticles interact inducing near-IR absorption. Therefore, a higher concentration of aggregated nanoparticles is needed for near-IR responsive nanocontainers. With a surface density of less than 50%, the temperature rise in the micrometer size volume was found to reach several degrees, so distributing nanoparticles in desired patterns is important.[28] The local temperature rise on nanoparticles can be rather high, over 100 degrees, and it can be controlled by the incident intensity and adjusted to just several degrees of temperature rise to induce release of encapsulated materials. Most importantly, the presence of absorption centers in the shell of a nanocontainer assures that the temperature rise occurs only locally in the vicinity of the nanoparticle; the temperature decreases rapidly on the nanometer scale, assuring that the surrounding environment is unaffected.[29] Also, the size of nanoparticles needs to be chosen comparable to the thickness of the polyelectrolyte multilayers. The average size of silver nanoparticles was ~8 nm, which is comparable to several layers of polyelectrolytes around the corrosion inhibitor.

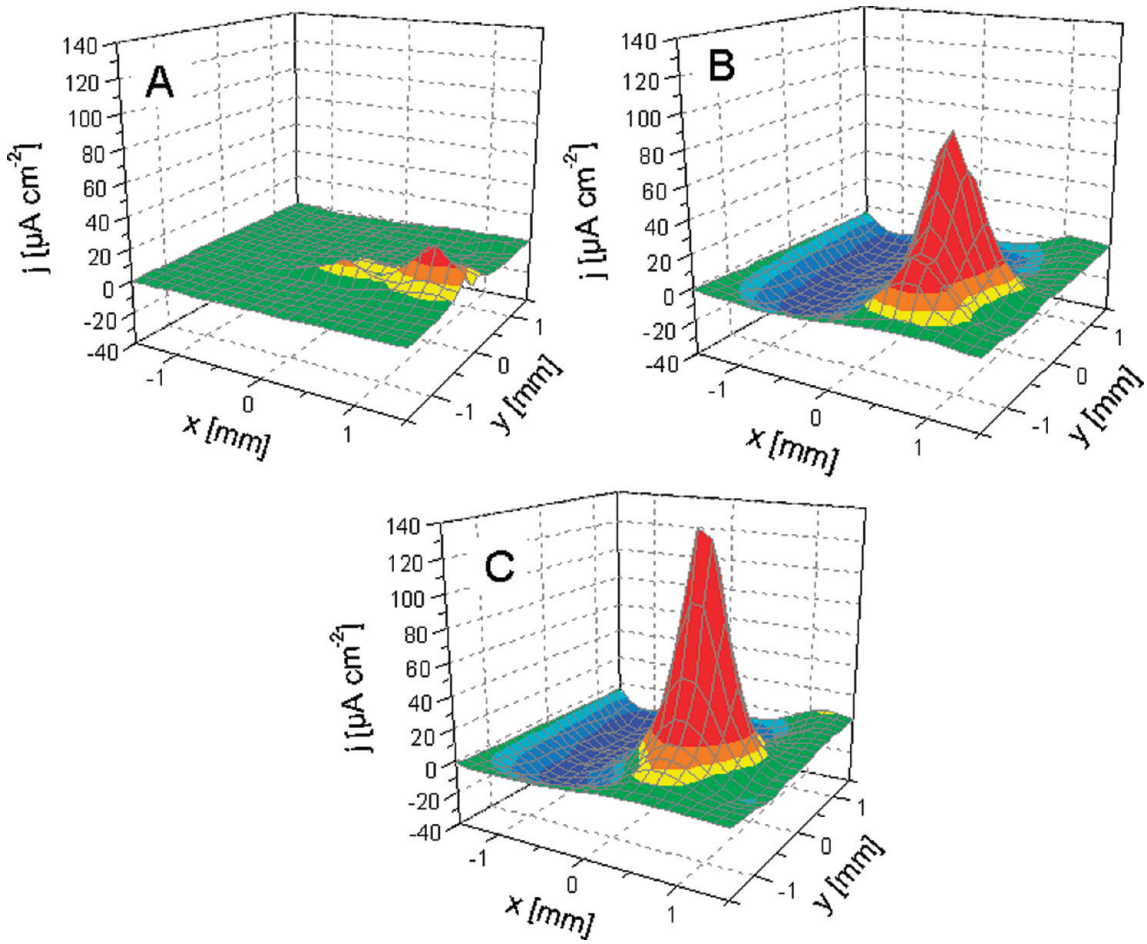

Figure 5. Scanning vibrating electrode measurements (SVET) of the ionic currents above the surface of individual sol−gel at (A) beginning moment; (B) 18 h of immersion; (C) 140 h of immersion. Scale units: µA · cm^{-2}, spatial resolution: 150 µm. Solution: 0.1 M NaCl.

The release characteristics of nanocontainers with successfully encapsulated benzotriazole were studied in aqueous neutral solutions under laser irradiation and, for comparison, under neutral or alkaline pH adjusted by addition of NaOH. As seen in Figure 4, nanocontainers exhibit spontaneous release of benzotriazole under laser irradiation. If one compares with pH-stimulated release of corrosion inhibitor, the laser-stimulated release occurs up to three times quicker. It should be noted that every corrosion process is accompanied by pH changes in the local corrosion area. The pH value can be reduced or increased depending on the nature of the corrosion process and the metallic substrate and could be used as an effective trigger to open the shell of the containers releasing the inhibitor into the corrosion pit and, as a consequence, to stop propagation of corrosion. In general, the application of the appropriate way of inhibitor release depends on the demands required from feedback active anticorrosion coatings. For coatings where the immediate release of the inhibitor is necessary, the use of nanocontainers, which could be immediately opened by laser irradiation, is a very important advantage.

The SVET technique permits the mapping of the current density in an electrolyte close to the substrate surface. The electrode vibrates and indicates the current flow in the electrolyte due to the corrosion processes occurring on the substrate surface. The measured current density vectors permit mapping of both the magnitude and direction of current flow immediately above the substrate surface. The SVET is thus capable of providing detailed spatially resolved information not readily obtainable by other techniques. The current density maps displayed in the normal or *z*-component of the measured current density in the plane of the vibrating electrode are plotted in 3D format over the scan area, with positive and negative current densities representing anodic and cathodic regions, respectively. The measurements with light-controllable anticorrosion coatings deposited onto aluminum alloy AA2024 were taken at the open-circuit potential. At least six specimens of each sample type were prepared and scanned to assess reproducibility of the observed phenomena.[40,41] SVET allows investigation of the termination of the corrosion process under IR laser irradiation. Figure 5 shows the current density maps for

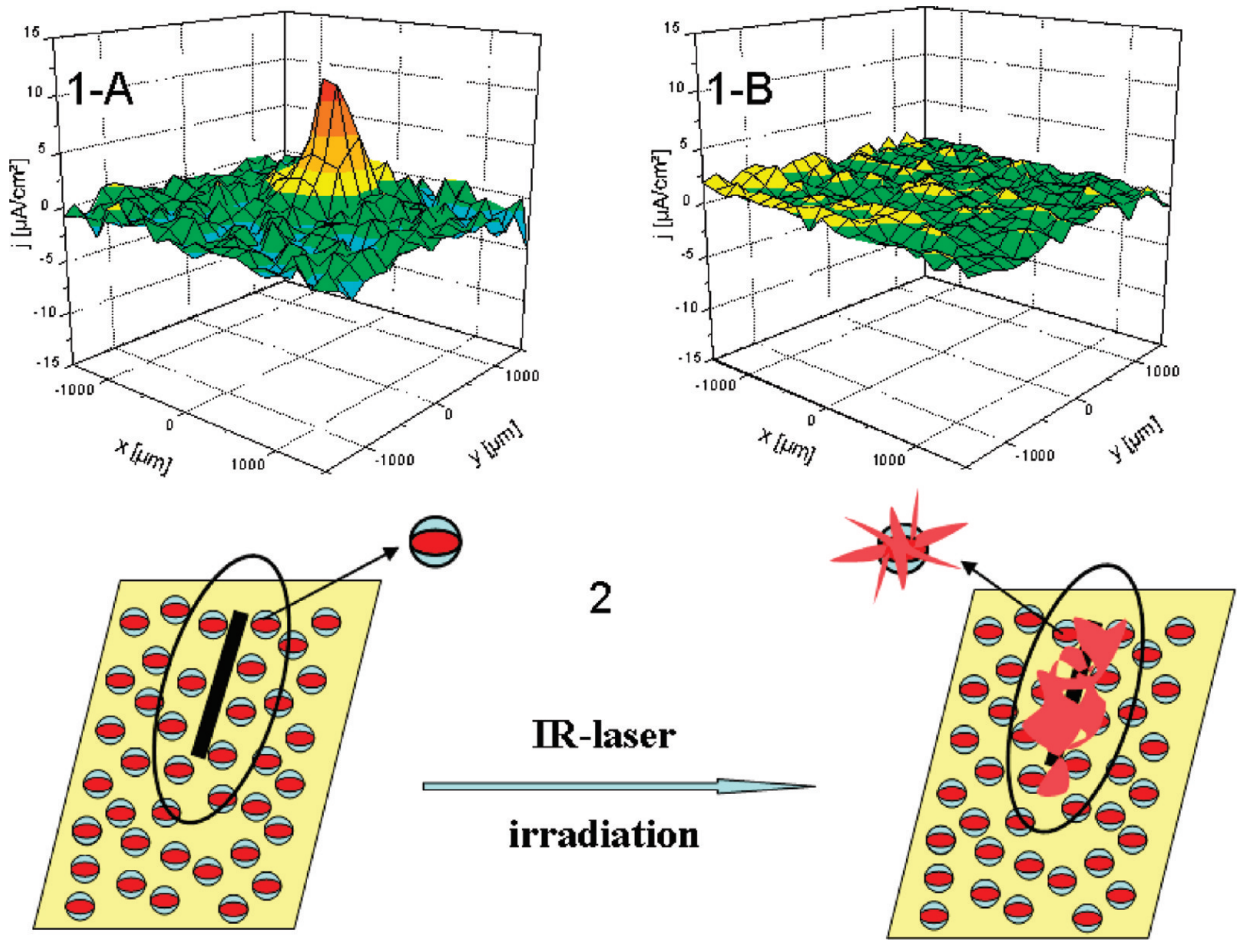

Figure 6. (1) Scanning vibrating electrode measurements (SVET) of the ionic currents above the surface of polyelectrolyte SiO_2 containers incorporated into SiO_x:ZrO_x sol−gel film (A) after 18 h immersion in 0.1 M NaCl; (B) after local laser irradiation of the corrosion area. Scale units: μA · cm^{-2}, spatial resolution: 150 μm. (2) Scheme of the inhibitor release after local laser irradiation explaining the healing of the defect.

sol−gel-coated aluminum alloy during the process of corrosion upon immersion in 0.1 M NaCl. A significant current flow was observed after 18 h of scanning time (Figure 5B) on the surface of the undoped sol−gel film. The anodic activity increases in time, which is seen from the higher corrosion activity in Figure 5C in comparison with Figure 5B. A regulation of the corrosion process could possibly occur by means of containers with corrosion inhibitor incorporated into the sol−gel film. Figure 6A shows the map recorded after 18 h of immersion of the sol−gel loaded with IR laser sensitive containers. In these experiments, the idea was to study the effect of the container opening under laser irradiation (and, consequently, the corrosion inhibitor release) on the corrosion process termination. It is seen from Figure 6B that immediately after irradiation the corrosion disappears. Thus, to achieve fast healing of the corrosion, it is preferable to use IR laser stimulated treatment of the corrosion centers. The scheme (Figure 6.2) shows how the healing of corrosion defect works: when the cracks appear and corrosion begins, one can achieve the release of corrosion inhibitor and defect healing using laser irradiation; moreover, in the absence of mechanical defects, these films ensure highly efficient corrosion protection.

In summary, in this study, submicrometer and nanosized laser-sensitive containers have been developed. The laser and pH-stimulated corrosion inhibitor release from the inner volume of polyelectrolyte containers was studied. It was shown that release under laser irradiation is faster, which allows achieving fast stimulated healing of corrosion defects after container incorporation into the silica−zirconia-based sol−gel matrix, which is confirmed by the scanning vibration electrode technique studies. These measurements permit visualization of the healing under laser irradiation. The release characteristics due to laser−nanoparticle interaction were analyzed. Temperature rise of just several degrees is sufficient for inducing release of encapsulated materials. Tuning the illumination wavelength, intensity of the incident laser beam, and concentration of nanoparticles makes the laser release method a rather versatile tool for corrosion protection.

EXPERIMENTAL SECTION

Materials. Aluminum alloy AA2024 was supplied by EADS Deutschland GmbH, polyethyleneimine (PEI, $M_w \sim 600\,000-1\,000\,000$), poly(sodium 4-styrenesulfonate) (PSS, $M_w \sim 70\,000$), HCl, NaCl, zirconium *n*-propoxide (TPOZ), 3-glycidoxypropyltrimethoxysilane (GPTMS), propanol, ethylacetoacetate, EtOH, tetraethoxysilane (TEOS), cetyltrimethylammonium bromide (CTAB), HNO_3, TiC, and $AgNO_3$ were purchased from Sigma-Aldrich and used without further purification. The water was purified in a three-stage Millipore Milli-Q Plus 185 purification system and had a resistivity higher than 18 MΩ/cm.

Preparation of Porous SiO_2 and TiO_2 Particles. SiO_2 mesoporous particles were produced using an aerosol-assisted self-assembly process. The reaction mixtures were prepared in reactors at 25 °C under stirring. The silica sources were added to the solutions under stirring to give gel mixtures with the molar composition TEOS/CTAB/NH_3/H_2O = 1:0.52:16:39. After droplet addition of TEOS, the mixture was heated until gel formation. Gels were then autoclaved at the desired temperature (70 °C) for 5 h under static conditions. The materials were recovered by filtration, washed with water, and oven-dried at 540 °C for 6 h (Figure 1(1-A)). The mesoporous titania was synthesized by oxidation of titanium carbide by 5 M nitric acid. The resultant particles were *ca.* 100 nm in size and have ~6−7 nm pores (Figure 1(1-B)). According to XRD analysis, the titania network was made of anatase crystallites with medium size of *ca.* 3 nm.

Nanocontainer Loading. Benzotriazole (Bt) was loaded inside the pore of the containers. For this purpose, dispersed particles were mixed with 10 mg/mL solution of benzotriazole. A vial containing the mixture was transferred to a vacuum jar and then repeatedly evacuated using a vacuum pump. Slight bubbling of the suspension indicates the air being removed from the container interior. After the bubbling was stopped, the vial was sealed for 30 min to reach equilibrium in benzotriazole distribution between the inner volume and the surrounding solution. The titania or silica suspension was centrifuged to remove excess of the dissolved benzotriazole and dried. The process was repeated four times to ensure the saturation of the inner titania cavity with precipitated benzotriazole. To produce the polyelectrolyte shell, we followed the LbL deposition procedure involving PEI and PSS polyelectrolyte molecules. The deposition of the positive PEI was performed on the first stage mixing 20 mL of SiO_2 or titania (15 or 12 wt %, respectively) colloidal solution with 3 mL of 2 mg/mL PEI solution for 15 min. Deposition of the negative PSS layer was carried out from 2 mg/mL PSS water solution. The same procedure was repeated twice. Washing of the resulting composite nanoparticles was performed by centrifugation after each adsorption step. The resulting nanocontainers have Bt-SiO_2/PEI/PSS/PEI/PSS and Bt-TiO_2/PEI/PSS/PEI/PSS structures. The benzotriazole content in the nanocontainers is equal to 75 mg/g of the initial SiO_2 particles and 69 mg/g of the initial TiO_2 particles.

Modification of the Containers by Fine Silver Particles. To make our containers sensitive to the laser irradiation, preformed silver nanoparticles were added to the container shell. In the case of mesoporous SiO_2-based containers, silver nanoparticles were incorporated directly into the polyelectrolyte shell (Figure 1(1-B)). For this purpose, silver particles were added into the polyelectrolyte solutions for layer-by-layer deposition. Thus, these noble metal particles were fixed between polyelectrolyte layers. In the case of titania-based containers, silver nanoparticles were photodeposited onto the titania core before the container loading with corrosion inhibitor and polyelectrolyte shell formation (Figure 1(2-B)). The nucleation of the metal phase at the semiconductor surface under illumination is a well-investigated process; in particular, it was studied as the process of latent image formation in the photocatalytic lithography.[22] By changing the deposition conditions (exposure dose, light intensity), the metal loading can be effectively controlled and the dispersity of the resultant metal nanophase can be readily varied in wide ranges. Silver nanoparticles were deposited onto the TiO_2 core by illumination of the TiO_2 surface with UV light (10 s) in aqueous solutions containing silver ions from 10^{-5} M $AgNO_3$.

Synthesis and Deposition of Sol−Gel Films. The hybrid zirconia−organosilica films loaded with titania or silica containers were prepared using the controllable sol−gel route by mixing in 1:2 volume ratio the following sols: (i) zirconia sol obtained by hydrolyzing 70 wt % zirconium *n*-propoxide in propanol mixed with ethylacetoacetate (1:1 volume ratio) and (ii) organosiloxane sol synthesized by hydrolyzing 3-glycidoxypropyltrimethoxysilane in isopropanol (in both cases acidified water pH = 1 was used to initiate the hydrolysis). The mesoporous titania or silica was added into the resulting mixture in an amount of 3 mg/mL. The container loaded SiO_x-ZrO_x films were deposited onto metal (aluminum alloy AA 2024) substrates by a dip-coating procedure; the rate of substrate withdrawal was 18 cm/min. After the coating, the samples were cured at 130 °C for 1 h (Figure 2).

Characterization. The morphology of titania and silica was investigated by scanning electron microscopy (SEM) (LEO-1420, Carl Zeiss, Germany) and transmission electron microscopy (TEM) (LEO 906 E, Carl Zeiss, Germany). The specific surface area of the silica and titania container cores was obtained by N_2 adsorption fitted with BET isotherms (Micrometrics, ASAP 2010). Atomic force microscopy (AFM, Nanoscope III Multimode AFM, Digital Instruments Inc., USA, operating in tapping mode) were used for characterization of the obtained particles and of the surface of SiO_x-ZrO_x film loaded with containers. AFM tips (PPP-NCH-W) having a resonance frequency of 302−354 kHz and a stiffness of 25−42 N/m were purchased from Nanosensors (Germany). Absorption spectra in the ultraviolet and visible (UV/vis) range were recorded to determine benzotriazole concentration during loading and release by means of an Agilent 8453 spectrophotometer (Agilent Technologies, USA). Confocal fluorescence measurements were conducted on a Leica TCS SP inverted confocal microscope system (Leica, Germany) equipped with a 100× and 40× oil immersion objective having a numerical aperture of 1.4 and 1.25, respectively. The corrosion healing efficiency of the coatings after IR laser irradiation was investigated by the scanning vibrating electrode technique (SVET, from Applicable Electronics, USA). The diameter of the Pt-blackened electrode tip is 20 μm, the peak-to-peak amplitude is 60 μm, and the vibration frequency is 655 Hz. An area of 4.5 × 4.5 mm^2 was scanned with a step width of 150 μm. The probe was 300 μm above the sample surface. The scans had a duration of *ca.* 15 min each and were repeated every 0.5 h. The SVET method yields current density maps over the selected surface of the sample, thus allowing the monitoring of local cathodic and anodic activity in the corrosion zones.

Opening of the Polyelectrolyte Containers. Opening of the polyelectrolyte/silver containers was performed in two modes. First, using a homemade laser setup in which a collimated pulsed laser (time duration 700 ps, and power 3 μJ, 820 nm) was focused onto the sample through a microscope objective, 100× magnification, and the images were recorded by a charge-coupled device camera connected to a computer. In the second mode, an unfocused CW frequency-doubled Nd:YAG laser (operating at 532 nm) with an average incident power up to 150 mW exposed the sample in direct illumination for ~30 s. The laser intensity was measured by a Newport-183 °C power meter.

Acknowledgment. The research was supported by the NanoFutur program of the German Ministry for Education and EU FP7 project "MUST" NMP3- CP-IP 214261-2, Research (BMBF), Basic Research Foundation of Belarus and Volkswagen Foundation (project "Formation of bifunctional coatings on metals based on self-locating nano- and microcontainers").

Supporting Information Available: Video corresponding to the online irradiation of SiO_2/silver container coating using a homemade laser setup in which a collimated pulsed laser (time duration 700 ps, and power 3 μJ, 820 nm) was focused onto the sample. The images presented in Figure 3(1-A,B) are first and last moments of video. This material is available free of charge *via* the Internet at http://pubs.acs.org.

REFERENCES AND NOTES

1. Vargel, C. Corrosion de l'aluminium. *Technique et Ingénérie Série Matériaux*; Dunod: Paris, 1999; 528 pp.

2. Breslin, C. B.; Treacy, G.; Carroll, W. M. Studies on the Passivation of Aluminium in Chromate and Molybdate Solutions. *Corros. Sci.* **1994**, *36*, 1143–1154.
3. Kending, M. W.; Davenport, A. J.; Isacs, H. S. The Mechanism of Corrosion Inhibition by Chromate Conversion Coatings from X-ray Absorption Near Edge Spectroscopy (XANES). *Corros. Sci.* **1993**, *34*, 41–49.
4. Sasaki, K.; Isaacs, H. S.; Levy, P. W. *Mechanism of Al Alloy Corrosion and the Role of Chromate Inhibitors: Fourth Annual Report*; Air Force Office of Scientific Research; Frankel, G. S. , Ed.;Contact No. F49620-96-I-0479, 2000; 99 pp.
5. Abel, M.-L.; Watts, J. F.; Digby, R. P. Influence of Process Parameters on The Interfacial Chemistry of Γ-GPS on Aluminium. Review. *J. Adhes.* **2004**, *80*, 291–312.
6. Newhard, N. In *Corrosion Coatings-Chromate and Non-Chromate Types*; Leidheiser, H., Ed.; Science Press: Princeton, NJ, 1979; pp 225−241.
7. Lund, C. J.; Murphy, P. D.; Plat, M. V. In *Silanes and Other Coupling Agents*; Mittal, K. L., Ed.; VSP: Utrecht, The Netherlands, 1992; pp 423−437.
8. Cho, S. H.; Andersson, H. M.; White, S. R.; Sottos, N. R.; Braun, P. V. Polydimethylsiloxane-Based Self-Healing Materials. *Adv. Mater.* **2006**, *18*, 997–1000.
9. Bonnel, K.; Le Pen, C.; Peabeare, N. E. I. S. Characterization of Protective Coatings on Aluminium Alloys. *Electrochim. Acta* **1999**, *44*, 4259–4267.
10. Wang, D.; Bierwagen, G. P. Sol−Gel Coatings on Metals For Corrosion Protection. *Prog. Org. Coat.* **2009**, *64*, 327–338.
11. Voevodin, N. N.; Balbyshev, V. N.; Donley, M. S. Investigation of Corrosion Protection Performance of Sol-Gel Coatings on AA2024-T3. *Prog. Org. Coat.* **2005**, *52*, 28–33.
12. Moutarlier, V.; Neveu, B.; Gigandet, M. P. Evolution of Corrosion Protection for Sol−Gel Coatings Doped with Inorganic Inhibitors. *Surf. Coat. Technol.* **2008**, *202*, 2052–2058.
13. Voevodin, N. N.; Grebasch, N. T.; Soto, W. S.; Arnold, F. E.; Donley, M. S. Potentiodynamic Evaluation of Sol−Gel Coatings with Inorganic Inhibitors. *Surf. Coat. Technol.* **2001**, *140*, 24–28.
14. Zheludkevich, M. L.; Serra, R.; Montemor, M. F.; Yasakau, K. A.; Salvado, I. M. M.; Ferreira, M. G. S. Nanostructured Sol−Gel Coatings Doped with Cerium Nitrate as Pre-Treatments for AA2024-T3: Corrosion Protection Performance. *Electrochim. Acta* **2005**, *51*, 208–217.
15. Skorb, E. V.; Fix, D.; Andreeva, D. V.; Shchukin, D. G. Möhwald, H. Surface Modified Mesoporous SiO_2 Containers for Corrosion Protection. *Adv. Funct. Mater.* DOI: 10.1002/adfm.200801804.
16. Zheludkevich, M. L.; Serra, R.; Montemor, M. F.; Ferreira, M. G. S. Oxide Nanoparticle Reservoirs for Storage and Prolonged Release of the Corrosion Inhibitors. *Electrochem. Commun.* **2005**, *7*, 836–840.
17. White, S. R.; Sottos, N. R.; Geubelle, P. H.; Moore, J. S.; Kessler, M. R.; Sriram, S. R.; Brown, E. N.; Viswanathan, S. Autonomic Healing of Polymer Composites. *Nature* **2001**, *409*, 794–797.
18. Skirtach, A. G.; Munoz Javier, A.; Kreft, O.; Köhler, K.; Piera Alberola, A.; Möhwald, H.; Parak, W. J.; Sukhorukov, G. B. Laser-Induced Release of Encapsulated Materials Inside Living Cells. *Angew. Chem., Int. Ed.* **2006**, *45*, 4612–4617.
19. Skirtach, A. G.; Antipov, A. A.; Shchukin, D. G.; Sukhorukov, G. B. Remote Activation of Capsules Containing Ag Nanoparticles and IR Dye by Laser Light. *Langmuir* **2004**, *20*, 6988–6992.
20. Radziuk, D.; Shchukin, D. G.; Skirtach, A.; Möhwald, H.; Sukhorukov, G. Synthesis of Silver Nanoparticles for Remote Opening of Polyelectrolyte Microcapsules. *Langmuir* **2007**, *23*, 4612–4617.
21. El-Daly, S. A.; Gaber, M.; Al-Shihry, S. S.; El Sayed, Y. S. Photophysical Properties, Excitation Energy Transfer and Laser Activity of 3-(4′-Dimethylaminophenyl)-1-(2-pyridinyl) prop-2-en-1-one (DMAPP): A New Potential Laser Dye. *J. Photochem. Photobiol. A* **2008**, *195*, 89–98.
22. Skorb, E. V.; Ustinovich, E. A.; Kulak, A. I.; Sviridov, D. V. Photocatalytic Activity of Tio_2:In_2O_3 Nanocomposite Films towards the Degradation of Arylmethane and Azo Dyes. *J. Photochem. Photobiol. A* **2008**, *193*, 97–102.
23. Decher, G. Fuzzy Nanoassemblies: Toward Layered Polymeric Multicomposites. *Science* **1997**, *277*, 1232–1237.
24. Ibarz, G.; Dahre, L.; Donath, E.; Möhwald, H. Smart Micro- and Nanocontainers for Storage, Transport, and Release. *Adv. Mater.* **2001**, *13*, 1324–1327.
25. Antipov, A.; Sukhorukov, G. B. Polyelectrolyte Multilayer. Capsules as Vehicles with Tunable Permeabilitiy. *Adv. Colloid Interface Sci.* **2004**, *111*, 49–61.
26. Möhwald, H.; Donath, E.; Sukhorukov, G. B. Sequential Assembly of Nanocomposite Materials. In *Multilayer Thin Films. Sequential Assembly of Nanocomposite Materials*; Decher, G., Schlenoff, J. B., Eds.; Wiley-VCH: Weinheim, Germany, 2002; pp 363−392.
27. Shchukin, D. G.; Sukhorukov, G. B. Nanoparticle Synthesis in Engineered Organic Nanoscale Reactors. *Adv. Mater.* **2004**, *16*, 671–682.
28. Skirtach, A. G.; Dejugnat, Ch.; Braun, D.; Susha, A. S.; Rogach, A. L.; Parak, W. J.; Möhwald, H.; Sukhorukov, G. B. The Role of Metal Nanoparticles in Remote Release of Encapsulated Materials. *Nano Lett.* **2005**, *5*, 1371–1377.
29. Skirtach, A. G.; Déjugnat, C.; Braun, D.; Susha, A. S.; Rogach, A. L.; Sukhorukov, G. B. Nanoparticles Distribution Control by Polymers: Aggregates *versus* Nonaggregates. *J. Phys. Chem. C* **2007**, *111*, 555–564.
30. Kreibig, U. *Physics and Chemistry of Finite Systems: From Clusters to Crystals*; Jenna, P., Khanna, S. N., Rao, B. K., Eds.; Kluwer Academic Publishers: London, 1991.
31. Kreibig, U.; Schmitz, B.; Breuer, H. D. Separation of Plasmon-Polariton Modes of Small Metal Particles. *Phys. Rev. B* **1987**, *36*, 5027–5030.
32. Kahlau, T.; Quinten, M.; Kreibig, U. Extinction and Angle-Resolved Light Scattering from Aggregated Metal Clusters. *Appl. Phys. A: Mater. Sci. Process.* **1996**, *62*, 19–27.
33. Lu, L.; Capek, R.; Kornowski, A.; Gaponik, N.; Eychmüller, A. Selective Fabrication of Ordered Bimetallic Nanostructures with Hierarchical Porosity. *Angew. Chem., Int. Ed.* **2005**, *117*, 6151–6155.
34. Morikawa, M.; Kimizuka, N. Spatially Controlled Self-Assembly of Gold Nanoparticles Encased in α-Helical Polypeptide Nanospheres. *Chem. Commun.* **2005**, *38*, 4866–4868.
35. Zhang, G.; Wang, D. Y.; Möhwald, H. Decoration of Microspheres with Gold Nanodots-Giving Colloidal Spheres Valences. *Angew. Chem., Int. Ed.* **2005**, *117*, 7945–7948.
36. Radt, B.; Smith, T. A.; Caruso, F. Optically Addressable Nanostructured Capsules. *Adv. Mater.* **2004**, *16*, 2184–2189.
37. Holmin, R. E.; Ismagilov, R. F.; Haag, R.; Mujica, V.; Ratner, M. A.; Rampi, M. A.; Whitesides, G. M. Correlating Electron Transport and Molecular Structure in Organic Thin Films. *Angew. Chem., Int. Ed.* **2001**, *113*, 2378–2382.
38. Zhang, J.; Lahtinen, R. M.; Kontturi, K.; Unwin, P. R.; Schiffrin, D. J. Electron Transfer Reactions at Gold Nanoparticles. *Chem. Commun.* **2001**, *18*, 1818–1819.
39. Klitzing, R.; Möhwald, H. Proton Concentration Profile in Ultrathin Polyelectrolyte Films. *Langmuir* **1995**, *11*, 3554–3559.
40. He, J.; Gelling, V. J.; Tallman, D. E.; Bierwagen, G. P. A Scanning Vibrating Electrode Study of Chromated-Epoxy Primer on Steel and Aluminum. *J. Electrochem. Soc.* **2000**, *147*, 3661–3667.
41. He, J.; Gelling, V. J.; Tallman, D. E.; Bierwagen, G. P.; Wallacec, G. G. Conducting Polymers and Corrosion III. A Scanning Vibrating Electrode Study of Poly(3-octyl pyrrole) on Steel and Aluminum. *J. Electrochem. Soc.* **2000**, *147*, 3667–3673.